Miner Deposita (2006) 41:637–644
DOI 10.1007/s00126-006-0091-5

LETTER

SHRIMP U–Pb dating of the Antucoya porphyry copper deposit: new evidence for an Early Cretaceous porphyry-related metallogenic epoch in the Coastal Cordillera of northern Chile

Victor Maksaev · Francisco Munizaga · Mark Fanning · Carlos Palacios · José Tapia

Received: 15 May 2006 / Accepted: 23 August 2006 / Published online: 23 September 2006

Abstract The Antucoya porphyry copper deposit (300 Mt at 0.45% total Cu) is one of the largest deposits of a poorly known Early Cretaceous porphyry belt in the Coastal Cordillera of northern Chile. It is related to a succession of granodioritic and tonalitic porphyritic stocks and dikes that were emplaced within Jurassic andesitic rocks of the La Negra Formation immediately west of the N–S trending sinistral strike-slip Atacama Fault Zone. New zircon SHRIMP U–Pb data indicate that the porphyries of Antucoya crystallized within the time span from 142.7± 1.6 to 140.6±1.5 Ma (±2 σ), and late, unmineralized, NW–SE trending dacite dikes with potassic alteration and internal deformation crystallized at 141.9±1.4 Ma. The Antucoya porphyry copper system appears to be formed after a change of stress conditions along the magmatic arc from extensional in the Late Jurassic to transpressive during the Early Cretaceous and provides support for an Early Cretaceous metallogenic episode of porphyry-type mineralization along the Coastal Cordillera of northern Chile.

Keywords Porphyry copper · Andes · Chile · Geochronology · SHRIMP U–Pb dating · Coastal Cordillera

Editorial handling: B. Lehmann

V. Maksaev (✉) · F. Munizaga · C. Palacios
Departamento de Geología, Universidad de Chile,
Casilla 135128, Correo 21,
Santiago, Chile
e-mail: vmaksaev@ing.uchile.cl

M. Fanning
Research School of Earth Sciences,
Australian National University,
Canberra ACT 0200, Australia

J. Tapia
Sociedad Química y Minera de Chile,
Aníbal Pinto 3228,
Antofagasta, Chile

Introduction

The Antucoya porphyry copper deposit is one of the largest systems of the poorly known Early Cretaceous metallogenic belt in northern Chile (Camus 2003; Sillitoe and Perelló 2005), containing resources of 300 million tonnes of oxidized ore at 0.45% total Cu. The deposit is located 130 km NNE of Antofagasta, at 1,710 m of altitude on a subdued part of the Buey Muerto hills, on the eastern slope of the Coastal Cordillera (Fig. 1). Most geological information is from exploration work, including 43,000 m of diamond drilling and 510 m of underground galleries, done by SQM Metales S.A., the former owner of the property (Tapia et al. 1998). Recently, in December 2005, Antofagasta Minerals S.A. have acquired the Antucoya mining property and this company also holds the adjacent Buey Muerto claims, where a porphyry copper deposit with a geological resource of 219 Mt of oxide ore at 0.36% Cu was discovered (Perelló et al. 2003).

We have used zircon U–Pb dating to resolve a precise age of crystallization for three samples from the main intrusive rock units of the Antucoya porphyry copper deposit, and compared these results to other geochronological data, providing support for an Early Cretaceous metallogenic epoch in the Coastal Cordillera of northernmost Chile.

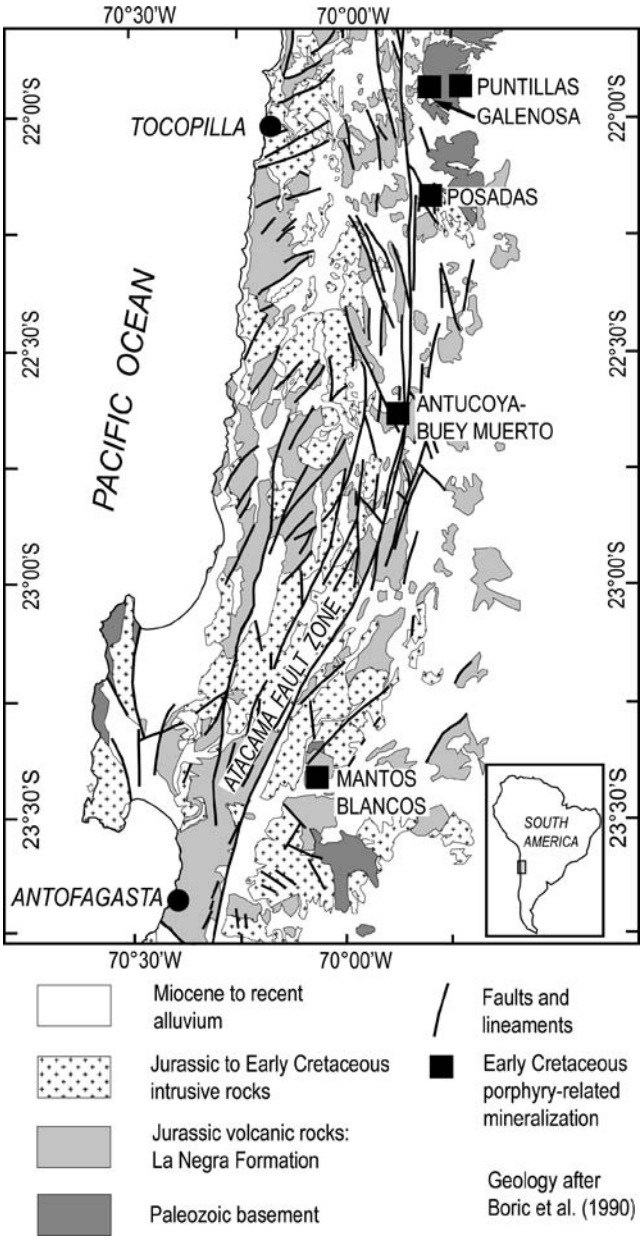

Fig. 1 Location of the Antucoya porphyry copper deposit and the geological setting of the Early Cretaceous porphyry-related copper deposits of the Coastal Cordillera of northern Chile

Geologic background

A variety of copper deposits, including iron oxide–copper–gold, VMS, strata-bound copper–(silver), and some porphyry copper deposits, represent an Early Cretaceous metallogenic episode along the Coastal Cordillera from Peru to central Chile (e.g., Maksaev and Zentilli 2002; Camus 2003; Sillitoe 2003; Sillitoe and Perelló 2005). Although exact ages are somewhat equivocal (Munizaga et al. 1985; Boric et al. 1990), the Early Cretaceous porphyry copper deposits represent the earliest mineralization of this type in the evolution of the Chilean Andes.

The Antucoya porphyry copper deposit occurs within an intrusive complex composed of multiphase granodioritic and tonalitic porphyries and dacite dikes, which were emplaced within Jurassic andesitic volcanic rocks of the La Negra Formation. Postmineralization gravel partly cemented by nitrates, regolith, and gypcrete cover most of the Antucoya deposit; thus, only limited surface exposure exists. Copper-bearing ore occurs as stockwork, dissemination, impregnation in altered rocks, and as breccia matrix; it is hosted by the granodioritic and tonalitic porphyries, and by magmatic to hydrothermal breccias, within an area of 1.6×1.0 km (Fig. 2). Unmineralized, NW-striking dacite dikes (5 to 20 m thick) crosscut the mineralized porphyries and hydrothermal breccias. The volcanic succession exposed at the Buey Muerto hills strikes 25–30°W and dips from 20 to 30°NE. It is formed out of massive aphanitic to porphyritic andesites, locally interbedded with fine-grained, tuffaceous calcareous sandstone and siltstone horizons. The Antucoya copper deposit occurs immediately west of a conspicuous N–S lineament of the main trace of the Atacama Fault Zone. This is a regional intraarc, sinistral strike-slip fault zone, which was active during the Early Cretaceous (e.g., Dallmeyer et al. 1996; Scheuber and Andriessen 1990). Dike emplacement and brecciation at Antucoya are controlled by NW-striking faults. These NW faults splay from the neighboring N–S Atacama Fault Zone and are consistent with a NW–SE compression at the time of faulting and dike emplacement.

Two altered and mineralized porphyry intrusions occur at Antucoya. The dominant lithology is granodioritic porphyry ("Antucoya porphyry") and lesser tonalite porphyry (known as "fine-grained porphyry"). The granodioritic porphyry is formed by plagioclase phenocrysts (25%) up to 3 mm long, and perthitic K-feldspar phenocrysts up to 1 mm long (5%). Plagioclase phenocrysts are altered to kaolinite, illite, calcite, and traces of anhydrite. The groundmass (70%) is a microcrystalline aggregate of quartz and argillized feldspar, with chlorite and opaque mineral dissemination and minor relicts of chloritized fine-grained biotite. The granodiorite porphyry contains a dense stockwork of quartz veinlets, some with oxidized copper minerals (atacamite, brochantite, chrysocolla, and copper wad), hematite, and limonites (after sulfides), and some with late veins of calcite, anhydrite, and opaque minerals.

The tonalite porphyry (fine-grained porphyry) has minor relict (phantom) plagioclase phenocrysts (ca. 10%) up to 2 mm long, with strong argillic alteration and partly calcite replacement. The groundmass (90%) is a microcrystalline aggregate of quartz and argillized plagioclase with abundant chlorite and disseminated opaque minerals that appear to completely replace mafic minerals and relicts of partly

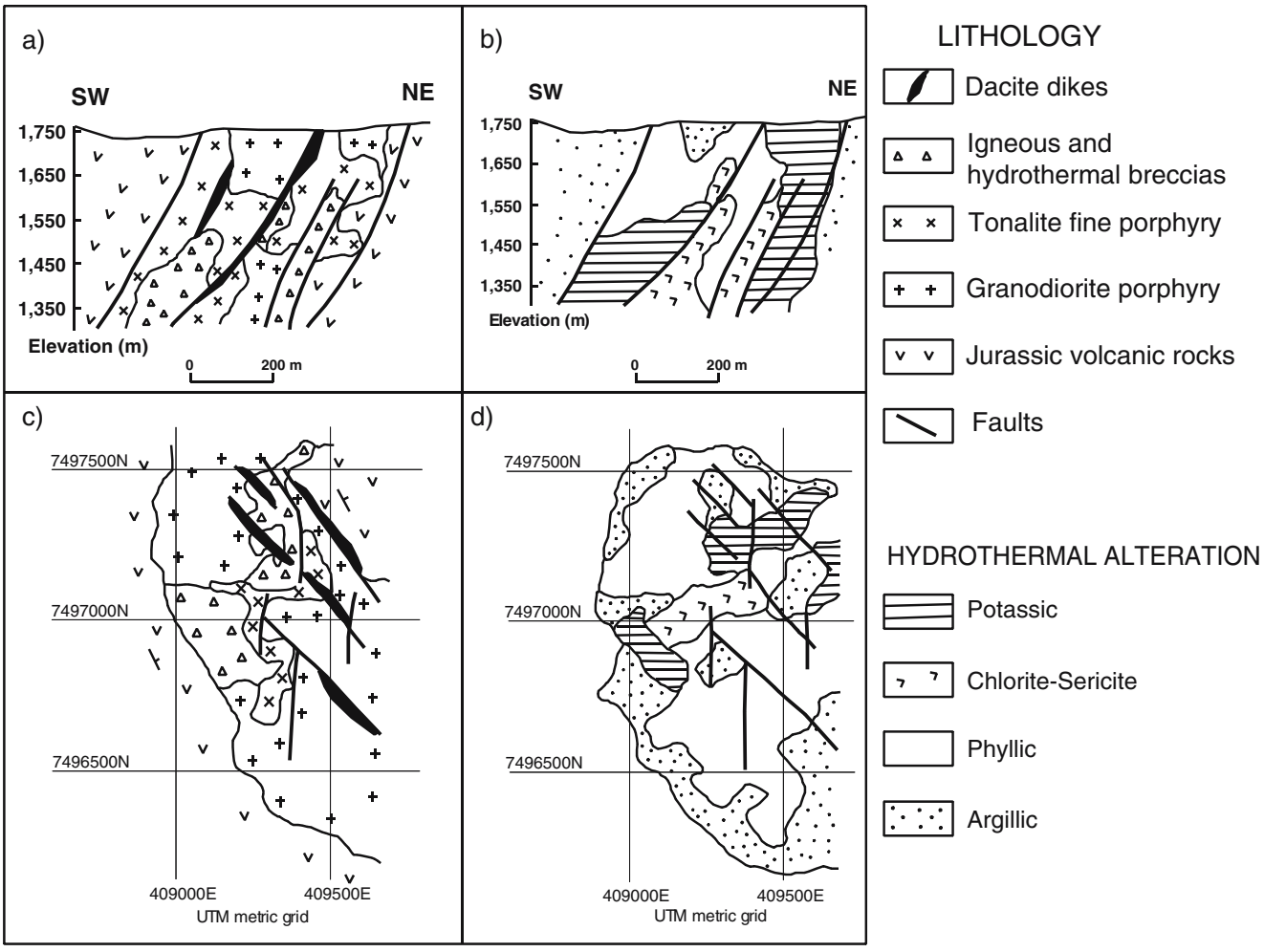

Fig. 2 Geology and hydrothermal alteration of the Antucoya porphyry copper deposit: **a** geological cross-section of the deposit, **b** cross-section showing the distribution of the hydrothermal alteration types, **c** geology of the 1,350-m level, and (**d**) hydrothermal alteration types of the 1,350-m level

chloritized microcrystalline aggregates of biotite and minor sericite. This porphyry also contains a stockwork of quartz veinlets, and late calcite veins, but also fractures coated by limonite and copper oxide minerals. The granodiorite and tonalite porphyries have mutual intrusion relationships, suggesting either that these are composite intrusions or that they intruded almost simultaneously. In addition, magmatic-hydrothermal breccias occur along the contacts between these two porphyries in the center of the deposit, but are also spatially related to NW-striking faults. These are polymictic and matrix-supported, pipe-like, irregular bodies, which range from near vertical to SW-dipping; their recognized vertical extent is 250 to 350 m. The uppermost part of the breccia bodies (above the 1,400-m level) has a matrix of hydrothermal minerals, whereas downward an altered granodioritic igneous matrix dominates. The breccia fragments are angular to subrounded and are composed of altered and mineralized granodioritic and tonalitic porphyries.

NW-striking, unmineralized, dark-gray dacite porphyry dikes crosscut the mineralized porphyries; these dacite dikes are formed by plagioclase phenocrysts (25%) up to 4 mm long, fresh or partly sericitized, and some affected by brittle microfracturing, partly chloritized microcrystalline biotite and opaque minerals forming pseudomorphs after amphibole phenocrysts (5%), and scarce quartz eyes up to 2 mm in diameter. The groundmass (70%) consists of microcrystalline aggregates of quartz and argillized plagioclase microliths. Fine-grained biotite dissemination occurs in the groundmass, but biotite is largely replaced by chlorite. Although the dacite dikes were intruded after mineralization, they are affected by potassic alteration (biotite), with partial chloritization and argillic overprint. These dacite dikes occur along NW-trending faults, and are internally affected by microfractures; this brittle deformation is probably related to fault reactivations after dike emplacement.

Table 1 Zircon SHRIM U–Pb data for intrusive rocks from Antucoya porphyry copper deposit

Grain spot	U (ppm)	Th (ppm)	Th/U	$^{206}Pb^{*}$ (ppm)	$^{204}Pb/^{206}Pb$	±	f_{206} %	Total				Radiogenic		Age (Ma)	
								$^{238}U/^{206}Pb$	±	$^{207}Pb/^{206}Pb$	±	$^{206}Pb/^{238}U$	±	$^{206}Pb/^{238}U$	±
Sample KP 64 granodiorite porphyry[a]															
1.1	29	15	0.51	0.6	0.002636	0.001160	2.52	44.56	1.07	0.0689	0.0045	0.0219	0.0005	139.5	3.4
2.1	30	15	0.51	0.6	0.000789	0.000781	4.79	44.84	0.98	0.0869	0.0071	0.0212	0.0005	135.4	3.2
3.1	29	14	0.47	0.6	–	–	3.87	42.20	0.92	0.0797	0.0057	0.0228	0.0005	145.2	3.3
4.1	24	14	0.60	0.5	0.001298	0.001042	5.13	42.88	1.03	0.0897	0.0086	0.0221	0.0006	141.1	3.7
5.1	50	37	0.73	1.0	0.003997	0.001266	2.57	43.95	0.80	0.0693	0.0033	0.0222	0.0004	141.4	2.6
6.1	41	18	0.43	0.8	0.001047	0.000806	2.97	45.87	0.89	0.0724	0.0051	0.0212	0.0004	134.9	2.7
7.1	29	13	0.46	0.6	0.005822	0.001844	4.58	42.36	0.94	0.0854	0.0080	0.0225	0.0006	143.6	3.5
8.1	60	36	0.60	1.2	0.002058	0.000832	2.29	43.02	0.72	0.0671	0.0029	0.0227	0.0004	144.8	2.5
9.1	25	15	0.62	0.5	0.004194	0.001588	4.68	41.49	0.97	0.0862	0.0060	0.0230	0.0006	146.4	3.6
10.1	36	13	0.36	0.7	0.005456	0.001516	3.75	42.67	0.88	0.0788	0.0078	0.0226	0.0005	143.8	3.3
11.1	37	25	0.67	0.7	0.003341	0.001115	4.37	46.03	0.94	0.0834	0.0043	0.0208	0.0004	132.6	2.8
12.1	29	13	0.46	0.6	0.002492	0.001069	5.30	41.22	0.92	0.0912	0.0050	0.0230	0.0005	146.4	3.4
13.1	64	32	0.51	1.2	0.001528	0.000966	2.58	44.70	0.77	0.0694	0.0041	0.0218	0.0004	139.0	2.5
14.1	39	20	0.50	0.8	0.002156	0.000896	2.67	43.47	0.88	0.0701	0.0055	0.0224	0.0005	142.7	3.0
15.1	23	11	0.49	0.5	0.008487	0.002690	6.55	41.24	1.04	0.1010	0.0062	0.0227	0.0006	144.4	3.8
16.1	33	15	0.46	0.7	0.002180	0.001309	3.53	42.47	0.97	0.0771	0.0099	0.0227	0.0006	144.8	3.8
17.1	42	18	0.43	0.8	0.001552	0.000811	3.45	43.58	0.86	0.0763	0.0072	0.0222	0.0005	141.3	3.1
18.1	38	18	0.47	0.7	0.002868	0.001168	3.47	43.75	0.88	0.0764	0.0068	0.0221	0.0005	140.7	3.1
19.1	15	6	0.42	0.3	0.008540	0.004370	9.17	42.85	1.74	0.1217	0.0170	0.0212	0.0010	135.2	6.3
20.1	50	24	0.47	1.0	0.000702	0.000695	1.86	43.90	0.78	0.0637	0.0074	0.0224	0.0005	142.5	2.9
Sample KP 65 tonalite porphyry[b]															
1.1	68	47	0.70	1.3	0.000797	0.000330	2.28	45.24	0.75	0.0669	0.0026	0.0216	0.0004	137.8	2.3
2.1	26	12	0.46	0.5	0.003689	0.001307	5.96	42.49	1.02	0.0963	0.0069	0.0221	0.0006	141.1	3.6
3.1	45	27	0.59	0.9	0.003545	0.001255	1.76	44.98	0.85	0.0628	0.0044	0.0218	0.0004	139.3	2.7
4.1	41	33	0.81	0.8	0.001369	0.001031	3.69	45.06	1.75	0.0781	0.0041	0.0214	0.0008	136.3	5.3
5.1	40	21	0.52	0.8	0.006451	0.001793	3.75	43.33	0.88	0.0787	0.0041	0.0222	0.0005	141.6	2.9
6.1	37	19	0.51	0.7	0.002680	0.001014	3.63	43.90	0.89	0.0777	0.0057	0.0220	0.0005	140.0	3.0
7.1	33	13	0.40	0.6	0.004584	0.001385	4.15	44.58	1.59	0.0818	0.0058	0.0215	0.0008	137.1	5.0
8.1	34	21	0.60	0.7	0.001990	0.001347	3.77	43.38	1.35	0.0789	0.0043	0.0222	0.0007	141.4	4.4
9.1	52	23	0.44	1.0	0.002369	0.000896	1.92	44.34	1.22	0.0641	0.0031	0.0221	0.0006	141.0	3.9
10.1	18	8	0.44	0.4	0.003563	0.002756	8.24	44.16	1.21	0.1142	0.0105	0.0208	0.0006	132.6	4.1
11.1	24	11	0.45	0.5	0.004281	0.001750	5.85	41.47	1.02	0.0955	0.0071	0.0227	0.0006	144.7	3.8
12.1	115	75	0.66	2.1	0.001706	0.000515	1.17	45.82	0.65	0.0581	0.0024	0.0216	0.0003	137.6	2.0
13.1	19	8	0.39	0.4	0.007665	0.002870	6.10	42.05	1.09	0.0974	0.0114	0.0223	0.0007	142.4	4.3
14.1	33	16	0.47	0.7	0.002978	0.000995	3.88	43.39	0.95	0.0798	0.0081	0.0222	0.0005	141.2	3.4
15.1	26	12	0.44	0.5	0.002869	0.001531	5.10	44.48	1.05	0.0894	0.0055	0.0213	0.0005	136.1	3.4
16.1	72	47	0.66	1.4	0.002282	0.000942	1.82	42.62	0.69	0.0635	0.0037	0.0230	0.0004	146.8	2.4
17.1	16	7	0.47	0.3	0.007377	0.003087	8.47	41.55	1.14	0.1163	0.0117	0.0220	0.0007	140.5	4.4

Table 1 (continued)

Grain spot	U (ppm)	Th (ppm)	Th/U	$^{206}Pb^{*}$ (ppm)	$^{204}Pb/^{206}Pb$	±	f_{206} %	Total $^{238}U/^{206}Pb$	±	$^{207}Pb/^{206}Pb$	±	Radiogenic $^{206}Pb/^{238}U$	±	Age (Ma) $^{206}Pb/^{238}U$	±
18.1	71	35	0.49	1.4	0.001268	0.000651	1.94	43.66	0.69	0.0644	0.0037	0.0225	0.0004	143.2	2.4
19.1	49	23	0.46	1.0	0.000481	0.000476	3.25	42.75	0.82	0.0748	0.0037	0.0226	0.0004	144.3	2.8
20.1	59	35	0.59	1.2	0.001709	0.000690	1.95	43.34	0.72	0.0645	0.0028	0.0226	0.0004	144.2	2.4
Sample KP 67 dacite dike[c]															
1.1	42	21	0.51	0.8	–	–	2.46	44.76	0.83	0.0684	0.0055	0.0218	0.0004	139.0	2.7
2.1	76	40	0.53	1.4	0.004192	0.001018	3.39	45.69	1.01	0.0757	0.0028	0.0211	0.0005	134.9	3.0
3.1	64	51	0.79	1.3	0.001315	0.001180	1.96	43.47	0.71	0.0645	0.0027	0.0226	0.0004	143.8	2.4
4.1	95	85	0.89	1.8	0.000980	0.000713	2.03	45.71	0.66	0.0649	0.0037	0.0214	0.0003	136.7	2.1
5.1	49	36	0.74	1.0	0.001691	0.000669	2.70	42.57	0.75	0.0704	0.0079	0.0229	0.0005	145.7	3.0
6.1	17	8	0.48	0.4	0.002972	0.002549	5.76	42.63	1.83	0.0947	0.0064	0.0221	0.0010	141.0	6.1
7.1	54	28	0.52	1.1	0.002655	0.001028	2.37	42.71	0.74	0.0678	0.0031	0.0229	0.0004	145.7	2.6
8.1	87	59	0.67	1.7	0.001742	0.000551	1.67	44.96	0.68	0.0621	0.0024	0.0219	0.0003	139.5	2.1
9.1	38	29	0.75	0.7	0.002700	0.001096	3.85	45.41	0.89	0.0793	0.0040	0.0212	0.0004	135.1	2.7
10.1	78	54	0.69	1.5	0.001284	0.000768	1.72	43.70	0.68	0.0626	0.0036	0.0225	0.0004	143.4	2.3
11.1	134	134	1.00	2.6	0.001037	0.000328	1.29	44.91	0.61	0.0591	0.0018	0.0220	0.0003	140.2	1.9
12.1	41	27	0.64	0.8	0.001173	0.000857	3.26	43.71	0.83	0.0748	0.0049	0.0221	0.0004	141.1	2.8
13.1	54	32	0.60	1.0	0.002813	0.000890	2.86	44.34	0.79	0.0716	0.0033	0.0219	0.0004	139.7	2.5
14.1	43	23	0.53	0.8	0.001576	0.000678	3.59	43.80	0.82	0.0774	0.0038	0.0220	0.0004	140.4	2.7
15.1	42	18	0.44	0.8	0.001395	0.000839	3.21	43.48	1.48	0.0744	0.0046	0.0223	0.0008	141.9	4.9
16.1	76	38	0.51	1.5	0.002553	0.000683	1.67	43.83	0.69	0.0622	0.0025	0.0224	0.0004	143.0	2.3
17.1	23	13	0.56	0.5	0.008293	0.002848	6.51	42.72	1.02	0.1007	0.0098	0.0219	0.0006	139.5	3.8
18.1	48	24	0.49	1.0	0.001997	0.000755	1.94	41.92	0.76	0.0645	0.0031	0.0234	0.0004	149.1	2.7
19.1	17	9	0.54	0.3	0.004144	0.003327	6.79	42.62	1.15	0.1029	0.0095	0.0219	0.0007	139.5	4.1
20.1	78	42	0.54	1.5	0.001894	0.000878	1.28	43.61	0.67	0.0591	0.0024	0.0226	0.0004	144.3	2.3

Uncertainties given at the 1σ level on spot analyses.
Error in Temora reference zircon calibration was 0.36% for the analytical session (not included in above errors but required when comparing data from different mounts).
f_{206} % denotes the percentage of ^{206}Pb that is common Pb.
Correction for common Pb made using the measured $^{238}U/^{206}Pb$ and $^{207}Pb/^{206}Pb$ ratios following Tera and Wasserburg (1972) as outlined in Williams (1998).
The final age includes error in standard zircon and is ±2 σ
[a] Mean weighted age 142.7±1.6
[b] Mean weighted age 140.6±1.5
[c] Mean weighted age 141.9±1.4

Four hypogene hydrothermal alteration assemblages were recognized at Antucoya: potassic, chlorite–sericite, quartz–sericite, and propylitic. The first three alteration types affect the porphyries and breccias, whereas propylitic alteration is restricted to the volcanic country rocks (Arellano 2003). However, most of the recognized orebody is affected by pervasive supergene argillic alteration (illite, dickite, and kaolinite) and oxidation (atacamite, brochantite, chrysocolla, copper wad, jarosite, and limonite), which extend down to depths of 300 to 350 m from the surface, and are overprinted on previous hypogene alteration types. Supergene processes, albeit unconstrained, are thought to have developed during the formation of the Oligocene–Miocene coastal Tarapacá pediplain (Mortimer et al. 1974). Potassic alteration mainly affects breccia bodies and the tonalitic porphyry characterized by the biotite, K-feldspar, and quartz assemblage. Fluid inclusion data indicate that potassic alteration took place at temperatures around 450–500°C, with fluid salinities from 7 to 68wt% NaCl equivalent related to liquid–vapor phase separation (Arellano 2003). A stockwork of quartz veins with chalcopyrite, pyrite, and molybdenite with quartz–sericitic haloes occurs in the uppermost part of the deposit (Fig. 2), and an assemblage of chlorite, sericite, smectite, quartz, pyrite, and chalcopyrite occurs within the Antucoya granodiorite porphyry and magmatic-hydrothermal breccias. The propylitic assemblage of chlorite, quartz, albite, epidote, calcite, and pyrite occurs within the surrounding volcanic country rocks (Arellano 2003).

Materials and analytical methods

Zircon grains were separated from three samples of the main intrusive rock units at the Antucoya porphyry copper deposit following normal mineral separation procedures: crushing, desliming, and heavy liquid and paramagnetic separation. Handpicked, prismatic dipyramidal zircon crystals, from 50 to 250 μm long, were mounted in epoxy together with chips of the Temora and SL13 reference zircons, sectioned approximately in half and polished. Reflected and transmitted light photomicrographs were prepared for all zircons, as were cathodoluminescence (CL) scanning electron microscope images. The CL images were used to decipher the internal structures of the sectioned grains and to ensure that the ~20 μm of SHRIMP spot was wholly within a single age component within the sectioned grains. U–Th–Pb analyses were made using the SHRIMP II at the Research School of Earth Sciences, The Australian National University, Canberra, Australia, following procedures given in Williams (1998, and references therein). Each analysis consisted of six scans through the mass range with a Temora U–Pb reference grain analyzed for every three unknown analyses. The data were reduced using the SQUID Excel Macro of Ludwig (2001); U/Pb ratios were normalized relative to a value of 0.0668 for the Temora reference zircon, equivalent to an age of 417 Ma (see Black et al. 2003). Uncertainties in the U–Pb calibration was 0.36% for an analytical session. Uncertainties given for individual analyses (ratios and ages) are at the 1σ level (Table 1). Tera and Wasserburg (1972) concordia plots, probability density plots with stacked histograms, and weighted mean $^{206}Pb/^{238}U$ age calculations were carried out using ISOPLOT/EX (Ludwig 2003). Weighted mean $^{206}Pb/^{238}U$ ages were calculated and the uncertainties are reported as 95% confidence limits.

Geochronology

Samples of the granodioritic porphyry, tonalitic porphyry, and a dacite dike from the Antucoya porphyry copper were dated. The new zircon geochronologic results are summarized on Table 1, whereas $^{206}Pb/^{238}U$ ages (±2 σ) and representative U–Pb Tera–Wasserburg concordia plots are shown in Fig. 3.

Zircons from the mineralized granodiorite porphyry of the Antucoya orebody (KP-64; Fig. 3a) yielded a $^{206}Pb/^{238}U$ age of 142.7±1.6 Ma (16 analyzed spots). Zircons from the mineralized tonalite porphyry (KP-65; Fig. 3b) yielded a $^{206}Pb/^{238}U$ age of 140.6±1.5 Ma (18 analyzed spots). Zircons from a postmineralization dacite dike from Antucoya (KP-67; Fig. 3c) yielded a $^{206}Pb/^{238}U$ age of 141.9±1.4 Ma (16 analyzed spots). The relatively invariable Th/U ratios and their respective spot U–Pb ages (Table 1) are consistent with magmatic zircons, and no inherited components were detected. These characteristics together with the high closure temperature of zircon (e.g., Cherniak and Watson 2000) allow us to interpret the new U–Pb data as representative of the crystallization ages of the respective igneous rocks. The three new zircon U–Pb ages are statistically identical as they overlap within their analytical uncertainty (at ±2 σ level), indicating that a succession of magma injections took place at Antucoya within a short period of time that falls within the time span of analytical uncertainty of the SHRIMP U–Pb dating method.

Discussion

The zircon U–Pb data indicate that the succession of intrusions of Antucoya crystallized within the time span from 142.7±1.6 to 140.6±1.5 Ma. Late, NW–SE trending, dacite dikes with internal brittle and ductile deformation that crystallized at 141.9±1.4 Ma suggest that the porphyry

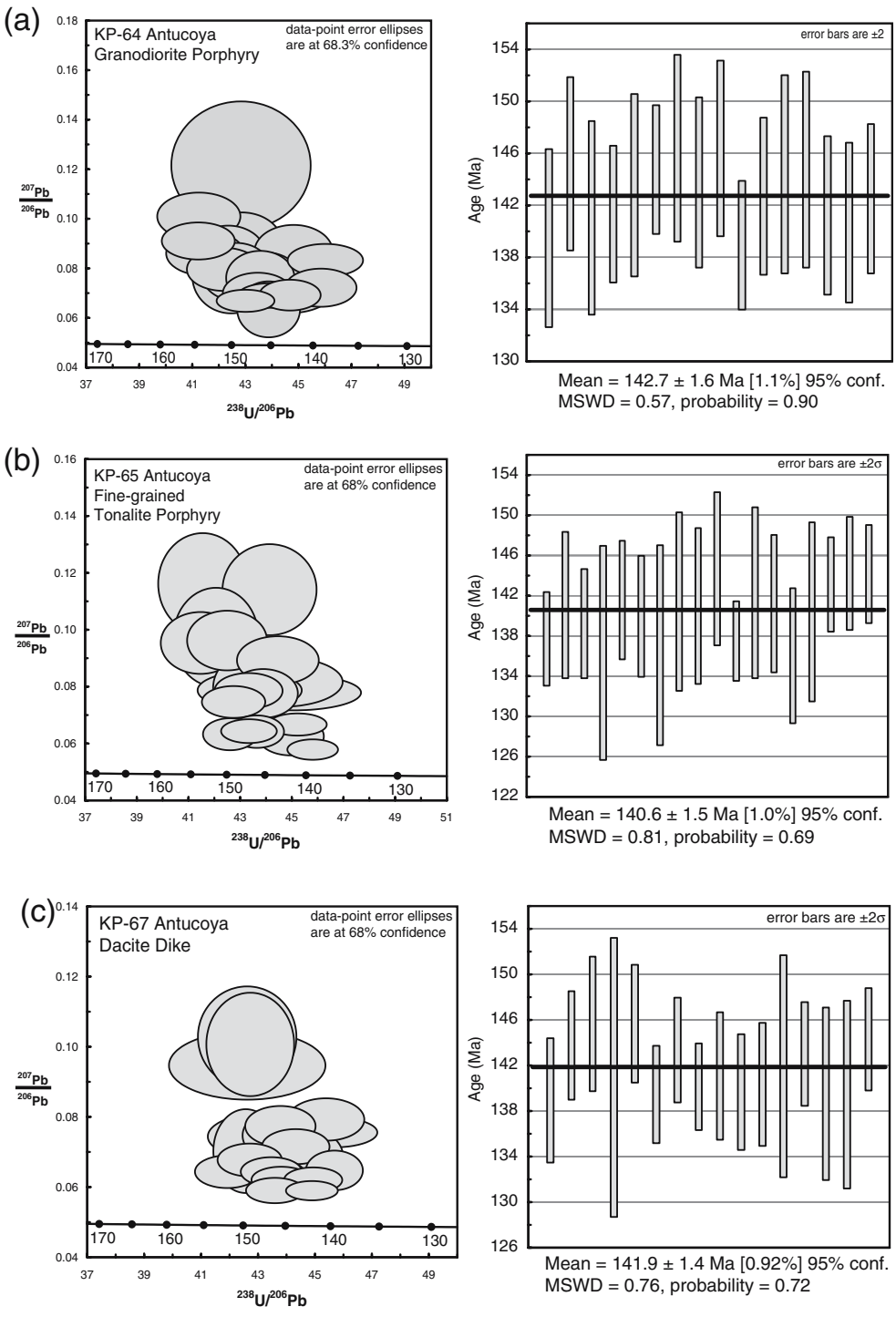

Fig. 3 Tera–Wasserburg concordia plot and weighted average age plot of SHRIMP U–Pb isotope data for **a** granodiorite porphyry (sample KP-64), **b** tonalite porphyry (sample KP-65), and **c** dacite dike (sample KP-67). Data are shown as 1 σ error ellipses; *error bars* and U–Pb ages are ±2 σ

system developed during a stage of active sinistral shearing along the neighboring N–S Atacama Fault Zone. The U–Pb age for a potassic altered, but unmineralized dike represents the minimum age for the hypogene copper mineralization. The formation of the Antucoya porphyry copper deposit is after a change of stress conditions along the Mesozoic magmatic arc from extensional in the Late Jurassic to transpressive during the Early Cretaceous, according to the tectonic interpretation of northern Chile by Scheuber and Gonzalez (1999).

Perelló et al. (2003) reported K–Ar ages of 137±4 Ma and 132±4 Ma for hydrothermal biotite and sericite, respectively, from the neighboring Buey Muerto property, which is part of the same porphyry copper system as

Antucoya. The biotite K–Ar age overlaps with the U–Pb ages within its relatively large analytical uncertainty, whereas the sericite age is slightly younger. However, these K–Ar ages are regarded as minimum age estimates for the porphyry system and are consistent with the lower closure temperature of micas for the K–Ar method compared to that of zircon in U–Pb dating.

Antucoya appears to be approximately coeval with the main mineralizing stage of the Mantos Blancos copper deposit, where hydrothermal breccias, disseminations, and stockwork sulfide mineralization were formed related to dioritic and granodioritic stocks and sills dated by the $^{40}Ar/^{39}Ar$ method between 141 and 142 Ma according to Ramírez et al. (2006). In addition, whole rock K–Ar ages of 132±8 Ma and 118±15 Ma were published for the Puntillas porphyry copper deposit (Munizaga et al. 1985; Boric et al. 1990). These ages also suggest an Early Cretaceous porphyry mineralization, but the large errors of the K–Ar ages make it uncertain if the Puntillas deposit was formed at the same time as Antucoya.

Conclusions

The Antucoya intrusive complex crystallized at 142.7±1.6 to 140.6±1.5 Ma, which is within a relatively short time span of less than ca. 2 Ma during the earliest Cretaceous. The emplacement of the porphyry intrusions took place within NW-trending faults that splay from the adjacent N–S sinistral strike-slip Atacama Fault Zone at the onset of transpression along the suprasubduction magmatic arc.

The U–Pb data for the Antucoya porphyry copper deposit provide the first precise ages for an early Cretaceous metallogenic episode of porphyry-type mineralization along the Coastal Cordillera of northern Chile. The same mineralizing episode appears to be represented by other porphyry copper deposits of northern Chile. However, more precise ages are required to check the temporal extent of the mineralizing event.

Acknowledgements This study was supported by CONICYT, Chile, through Fondecyt 1040492 grant to V. Maksaev and F. Munizaga (Universidad de Chile). We thank Massimo Chiaradia, Bernd Lehmann, and Carmen Holmgren for valuable reviews of the manuscript.

References

Arellano M (2003) Distribución y control de la mineralización del pórfido cuprífero Antucoya, II Región, Chile. B.Sc. thesis, Departamento de Geociencias Geológicas, Universidad Católica del Norte, Antofagasta, Chile, p 81

Black LP, Kamo SL, Allen CM, Aleinikoff JN, Davis DW, Korsch RJ, Foudolis C (2003) TEMORA 1: a new zircon standard for Phanerozoic U–Pb geochronology. Chem Geol 200:155–170

Boric R, Díaz F, Maksaev V (1990) Geología y yacimientos metalíferos de la Región de Antofagasta, Bol. 40. Servicio Nacional de Geología y Minería, Santiago, p 246

Camus F (2003) Geología de los sistemas porfíricos en los Andes de Chile. Servicio Nacional de Geología y Minería, Chile, p 267

Cherniak DJ, Watson EB (2000) Pb diffusion in zircon. Chem Geol 172:5–24

Dallmeyer RD, Brown M, Grocott J, Taylor GK, Treolar PJ (1996) Mesozoic magmatic and tectonic events within the Andean plate boundary zone, 26°–27°30′ S, North Chile: constraints from $^{40}Ar/^{39}Ar$ mineral ages. J Geol 104:19–40

Ludwig KR (2001) SQUID 1.02, a user's manual. Berkeley Geochronology Center, CA, special publication no. 2

Ludwig KR (2003) User's manual for Isoplot/Ex, version 3.0, a geochronological toolkit for Microsoft Excel. Berkeley Geochronology Center, CA, special publication no. 4

Maksaev V, Zentilli M (2002) Chilean strata-bound Cu–(Ag) deposits: an overview. In: Porter TM (ed) Hydrothermal iron oxide copper–gold and related deposits: a global perspective, vol. 2. PCG Publishing, pp 185–205

Mortimer C, Farrar E, Saric N (1974) K–Ar ages from tertiary lavas of the northernmost Chilean Andes. Geol Rundsch 63:484–490

Munizaga F, Huete C, Hervé F (1985) Geocronología K–Ar y razones iniciales $^{87}Sr/^{86}Sr$ de la Franja Pacífica de Desarrollos Hidrotermales, vol. 4. Actas IV Congreso Geológico Chileno, Antofagasta, pp 357–379

Perelló J, Martini R, Arcos R, Muhr R (2003) Buey Muerto: porphyry copper mineralization in the Early Cretaceous arc of northern Chile. Actas X Congreso Geológico Chileno, Concepción (electronic version)

Ramírez LE, Palacios C, Townley B, Parada MA, Sial AN, Fernandez-Turiel JL, Gimeno D, Garcia-Valles M, Lehmann B (2006) The Mantos Blancos copper deposit: an upper Jurassic breccia-style hydrothermal system in the Coastal Range of Northern Chile. Miner Deposita 41:246–258

Scheuber E, Andriessen PAM (1990) The kinematic and geodynamic significance of the Atacama fault zone, northern Chile. J Struct Geol 12:24–257

Scheuber E, Gonzalez G (1999) Tectonics of the Jurassic–Early Cretaceous magmatic arc of the north Chilean Coastal Cordillera (22–26°S): a story of crustal deformation along a convergent plate boundary. Tectonics 18:895–910

Sillitoe RH (2003) Iron oxide copper–gold deposits: an Andean view. Miner Deposita 38:787–812

Sillitoe RH, Perelló J (2005) Andean copper province: tectonomagmatic settings, deposit types, metallogeny, exploration, and discovery. In: Hedenquist JW, Thompson JFH, Goldfarb R, Richards J (eds) Economic geology one hundredth anniversary volume (1905–2005). Society of Economic Geologists, Littleton, Colorado, USA, p 845–890

Tapia J, Crespo H, Collao S (1998) Antucoya, pórfido cuprífero en la Cordillera de la Costa, II Región, Chile, vol. 3. In: Actas X Congreso Latinoamericano de Geología y VI Congreso Nacional de Geología Económica, Buenos Aires, Argentina, pp 250–255

Tera F, Wasserburg GJ (1972) U–Th–Pb systematics in three Apollo 14 basalts and the problem of initial Pb in lunar rocks. Earth Planet Sci Lett 14:281–304

Williams IS (1998) U–Th–Pb geochronology by ion microprobe. In: McKibben MA, Shanks III WC, Ridley WI (eds) Applications of microanalytical techniques to understanding mineralizing processes. Rev Econ Geol 7:1–35